Research Article

Journal of Environmental Nanotechnology

Moringa oleifera Extract-mediated Green Synthesis of Highly Active Ag@ZnO Nanohybrids for Azo Dye Removal

V. Subha[1], R. Kayalvizhi[2], R. Nagalakshmi[3], S. Kalpana[4] and M. Nagoor Meeran[5*]

[1]Department of Chemistry, R. M. D Engineering College, Tiruvallur, TN, India
[2]Department of Chemistry, Sri Eshwar College of Engineering, Coimbatore, TN, India
[3]Department of Humanities and Sciences (Chemistry), Aarupadai Veedu Institute of Technology, Vinayaka Mission's Research Foundation (DU), Chennai, TN, India
[4]Department of Computer Science, London South Bank University, Ajman, U.A.E
[5]Department of Chemistry, Vel Tech Rangarajan Dr. Sagunthala R&D Institute of Science and Technology (Deemed University), Chennai, TN, India
Received: 03.03.2026 Accepted: 13.04.2026 Published: 30.06.2026
*nagoorchem@gmail.com

ABSTRACT

In this work, the efficacy of *Moringa oleifera* flower extract-mediated synthesis of rod-like silver-decorated zinc oxide (Ag@ZnO) nanohybrids for the removal of the organic dye pollutant methyl orange (MO) from aqueous solutions was investigated. The nanohybrid was characterized using FE-SEM/EDX, FT-IR, XRD, and UV–Vis spectroscopic techniques. The nanohybrid effectively degraded methyl orange (MO) in the presence of $NaBH_4$ at room temperature. The results indicated that MO degradation efficiencies of 99.7%, 96.7%, and 97.2% were achieved within 10, 13, and 16 min, respectively. The enhanced performance was attributed to the synergistic effect between Ag and ZnO nanoparticles, which provided more active sites for improved catalytic degradation. Notably, the Ag@ZnO nanohybrid was synthesized via a green method using *M. oleifera* flower extracts without stabilizing agents, suggesting a sustainable approach. The findings highlight the potential of the nanohybrid for applications in environmental remediation and wastewater treatment, although further research is needed to fully explore its capabilities.

Keywords: Ag@ZnO nano hybrids; *Moringa oleifera*; Methyl orange; $NaBH_4$.

1. INTRODUCTION

Dye degradation has recently attracted a lot of attention due to the extensive use of synthetic dyes in several industries, such as textile, leather, cosmetics, and paper industries. When discharged into aquatic systems without adequate treatment, these pollutants provide significant hazards to human health and the environment owing to their toxicity, persistence, and non-biodegradable characteristics. Among various organic dyes, methyl orange (MO) is widely recognized as a representative azo dye because of its extensive industrial usage and high chemical stability. The existence of the –N=N– azo bond renders MO highly resistant to conventional degradation methods, thereby posing a major challenge in wastewater treatment (Xie *et al.*2021). Moreover, its unique absorption peak in the visible spectrum facilitates the efficient monitoring of deterioration behaviour by UV–Vis spectroscopy. Consequently, MO is frequently used as a model contaminant to evaluate the catalytic efficacy and practical applicability of newly synthesized nanomaterials. Conventional dye degradation methods combine biological and physicochemical processes (Donkadokula *et al.* 2020). Physical techniques such as adsorption and membrane filtration are widely used but often face challenges related to high operational costs and secondary pollution. Chemical methods, including coagulation, flocculation, and oxidation, can be effective; however, it releases harmful by-products(Rajeswaran *et al*. 2025a; Koul *et al.* 2022).

In recent years, metal nanoparticles (MNPs) have drawn much interest as heterogeneous catalysts due to their diverse uses across different industries. However, the widespread use of dyes and pigments in industrial processes poses a serious threat to aquatic ecosystems (Bavykina *et al.* 2020; Islam *et al.* 2022). Consequently, there is a pressing need for environmentally friendly approaches to mitigate pollution (Khanam *et al.* 2023). Combinations of MNPs with active inorganic metal oxides such as TiO_2, Fe_3O_4, CuO, zeolite, graphene oxide, and perlite have been explored as nanohybrids to address issues related to strength, stability, dissolution, and recovery (Janaki *et al.* 2025; Rajeswaran *et al.* 2025b).

Among them, Ag@ZnO nanohybrids have shown encouraging possibilities for the elimination of organic pollutants from water solutions due to their synergistic properties (Alzahrani *et al.* 2023). ZnO NPs are known for their cost-effectiveness (Sanjeev *et al.*

2023), versatility, and notable photocatalytic activity. Likewise, Ag NPs enhance catalytic performance through their excellent electron-transfer ability (Sharma *et al.* 2021; Khan *et al.* 2016). They also exhibit versatility, cost-effective synthesis, and exceptional optoelectronic properties, making them highly suitable for catalytic applications (Saleh *et al.* 2023). Synthesis methods for MNPs typically involve solvothermal, chemical reduction, and sol-gel methods, although these processes often come with high costs, chemical hazards, and environmental risks (Veeramalli *et al.* 2025; Parashar *et al.* 2020).

Recently, there has been a shift toward more sustainable synthesis routes that use water, biological extracts, biological systems, and microwave-assisted techniques (Venkatesh *et al.* 2024). These methods offer advantages such as clarity, cost-effectiveness, and environmental compatibility, which are particularly beneficial for biomedical and pharmaceutical applications (Meyyarasan *et al.* 2025). In recent studies, there is increasing interest in using extracts from natural sources, such as *M. oleifera* flowers, as reducing and stabilizing agents for synthesizing Ag@ZnO hybrids (Aththanayaka *et al.* 2023; Wafi and Mohammad, 2025; Kumar *et al.* 2025). *M. oleifera* is renowned for its bioactive compounds and eco-friendly nature, making it an ideal candidate for the sustainable synthesis of nanoparticles. The catalytic efficiency of the Ag@ZnO hybrid has been demonstrated in the absence of light, using sodium borohydride as a reducing agent (Sathish *et al.* 2021). In the presence of NaBH4, the catalytic reduction and decomposition of organic pollutants by metal nanoparticles occur via an electron-transfer process (Akhtar *et al.* 2020). Metal nanoparticles enhance this method by lowering the activation energy, making it more efficient. A significant redox difference between the electron donor (BH_4^- ion) and the acceptor (dye) influences electron transfer, contributing to the reaction's effectiveness (Uddin *et al.* 2020). Moreover, the catalytic reduction and decomposition of organic dye molecules by metal nanoparticles in the presence of NaBH4 is notably rapid and outperforms other methods by several orders of magnitude, which has led to its widespread recent adoption (Naz *et al.* 2021). This modern approach not only highlights the effectiveness of the Ag@ZnO hybrid in degrading organic pollutants under ambient conditions but also underscores the importance of green chemistry principles in developing environmentally benign catalysts (Usliyanage *et al.* 2025).

This study employed *Moringa oleifera* flower extract as a novel green precursor for the synthesis of Ag nanoparticles (Ag NPs), ZnO nanoparticles (ZnO NPs), and Ag@ZnO hybrid nanostructures. Compared to previously reported plant-mediated approaches, *Moringa oleifera* flower extract is abundant in several phytochemicals, such as flavonoids, phenolics, and proteins, which function concurrently as reducing and stabilizing agents, facilitating controlled growth and improved dispersion of nanoparticles. Furthermore, the development of the Ag@ZnO hybrid structure enhances interfacial interactions and synergistic effects, resulting in superior catalytic performance compared with the individual components. This study offers a sustainable and efficient method for designing high-performance nano catalysts for environmental remediation applications.

2. MATERIALS AND METHODS

2.1 Materials

Zinc nitrate pentahydrate ($Zn(NO_3)_2 \cdot 5H_2O$, ≥99.8%), silver nitrate ($AgNO_3$, ≥99.9%), methyl orange (MO), and sodium borohydride ($NaBH_4$) were purchased from Sigma-Aldrich, India, and used as received. All glassware and reagents were of analytical reagent (AR) grade and were used without further purification. Milli-Q water was used during the experiment. *M. oleifera* flowers were collected from Chennai, Tamil Nadu, India.

2.2 Development of Natural Surfactant Agent

A natural capping agent from *M. oleifera* flowers was prepared by finely grinding 10 g of dried flowers into a powder. The powder was refluxed in disinfected DI water at 90°C for 2h to extract bioactive compounds, preserving the plant-derived compounds' integrity. The liquid extract was then centrifuged at 6500 rpm to separate solid residues (Tashi *et al.*2016). The upper water-soluble extract contained natural compounds known for their effectiveness in nanoparticle synthesis, stabilizing and regulating the growth of nanomaterials.

2.3 Green Fabricated AgNPs and ZnO NPs

Green fabrication of Ag NPs using *M. oleifera* flower extract is a simple and efficient process. The extract of *M. oleifera* flower contains numerous bioactive phytochemicals, such as flavonoids, phenolic compounds, proteins, and reducing sugars, which are crucial for nanoparticle synthesis. These chemicals function as natural reducing agents by transferring electrons to metal ions (Ag^+ and Zn^{2+}), resulting in their transformation into matching nanoparticles. Moreover, functional groups including hydroxyl (–OH), carboxyl (–COOH), and amino ($–NH_2$) groups in these biomolecules facilitate the stability and capping of nanoparticles, thus averting agglomeration and improving their dispersion. To synthesize Ag NPs, an aqueous solution of silver precursor was mixed with *M. oleifera* flower extract with continuous stirring. The reaction mixture was held at 60 °C for 60 min, during which Ag^+ ions were reduced. The pH of the reaction

medium was observed to be roughly 7–8, which promoted effective reduction and stabilization of nanoparticles. The formation of Ag NPs was confirmed and monitored through UV–Vis spectroscopy, revealing a characteristic surface plasmon resonance (SPR) band of Ag NPs. This process typically occurs within 20 min (Uribe-Lopez *et al.*2021). Similarly, the precursor solution for ZnO nanoparticle synthesis was treated with floral extract and agitated constantly. The reaction was conducted at 70 °C for 2 h, and the pH of the solution was adjusted to approximately10 using a moderate base to facilitate the synthesis of ZnO NPs. The resultant precipitate was further washed and dried to produce pure ZnO nanostructures.

2.4 Construction of Ag@ZnO Hybrid Nanostructure

The Ag@ZnO hybrid nanostructure was constructed by dispersing the prepared ZnO NPS in the floral extract, followed by the addition of a silver precursor solution. The reaction mixture was held at 65 °C for 90 min with constant agitation. The pH of the medium used was maintained between 8 and 9, facilitating the deposition of Ag NPs onto the ZnO surface and leading to the development of the Ag@ZnO hybrid structure. After about 10 min, the solution's color transitioned from yellow to black as a result of SPR stimulation, indicating the creation of the nanocomposite (Arun*et al.*2025). The resulting solution is then centrifuged at 7000 rpm for 30 min, causing the Ag@ZnO hybrid to fully precipitate. Moreover, the precipitate was rinsed thrice with ethanol and air-dried for 24 h at ambient temperature.

2.5 Removal of MO Dye

The catalytic activity for the elimination of MO dye was investigated using Ag NPs, ZnO NPs, and Ag@ZnO hybrid in conjunction with $NaBH_4$(Bloch *et al.*2022). In a typical catalytic degradation experiment, 10 mg of the synthesized nano catalyst was added to 50 mL of methyl orange (MO) solution (10 mg L^{-1}) under continuous stirring. The reaction was initiated by the addition of 1 mL of freshly prepared $NaBH_4$ solution (0.1 M), and the degradation process was monitored at regular intervals. The synergistic effect of the NPs and NaBH4 facilitated the efficient reduction and breakdown of the MO dye. The percentage of catalytic reduction was computed:

$$Elimination\ (\%) = \frac{C - C_0}{C} \times 100 \qquad \ldots(1)$$

Where C represents the concentration of the control dye solution, and C_0 represents the concentration of the dye solution after treatment with nanomaterials.

3. RESULTS AND DISCUSSION

3.1 Formation Mechanism of Ag@ZnO Nanohybrids

The bio reduction of Ag^+ to Ag^0 using the phyto molecular constituents of *M. oleifera* flower extract involves its use as both a reducing and stabilizing agent for the sustainable and cost-effective synthesis ofAg@ZnO hybrids, as shown in Fig. 1(a). The extract contains flavonoids and phenolic acids, which are believed to reduce Ag^+ ions to Ag NPs, and also form ZnO NPs as well as stabilize them effectively. However, the stabilization occurs through hydrogen bonding and electrostatic interactions among the bioorganic moieties and the Ag@ZnO NPs (Zhang *et al.*2025). The weaker interaction of biomolecules with the nascent Ag-decorated ZnO nanocrystals may lead to isotropic crystal growth and the production of spherical-shaped Ag NPs and rod-shaped ZnO NPs. Antioxidants and polyphenols in the extract further aid in reducing Ag^+/Zn^{2+}ions, facilitating the formation of Ag@ZnOhybrid.The UV spectrum of the extract exhibited a band around 250 nm, indicating the presence of polyphenolic compounds that act as protective agents during nanoparticle formation and are associated with $\pi \rightarrow \pi^*$ transitions (Shahzadi *et al.*2025).

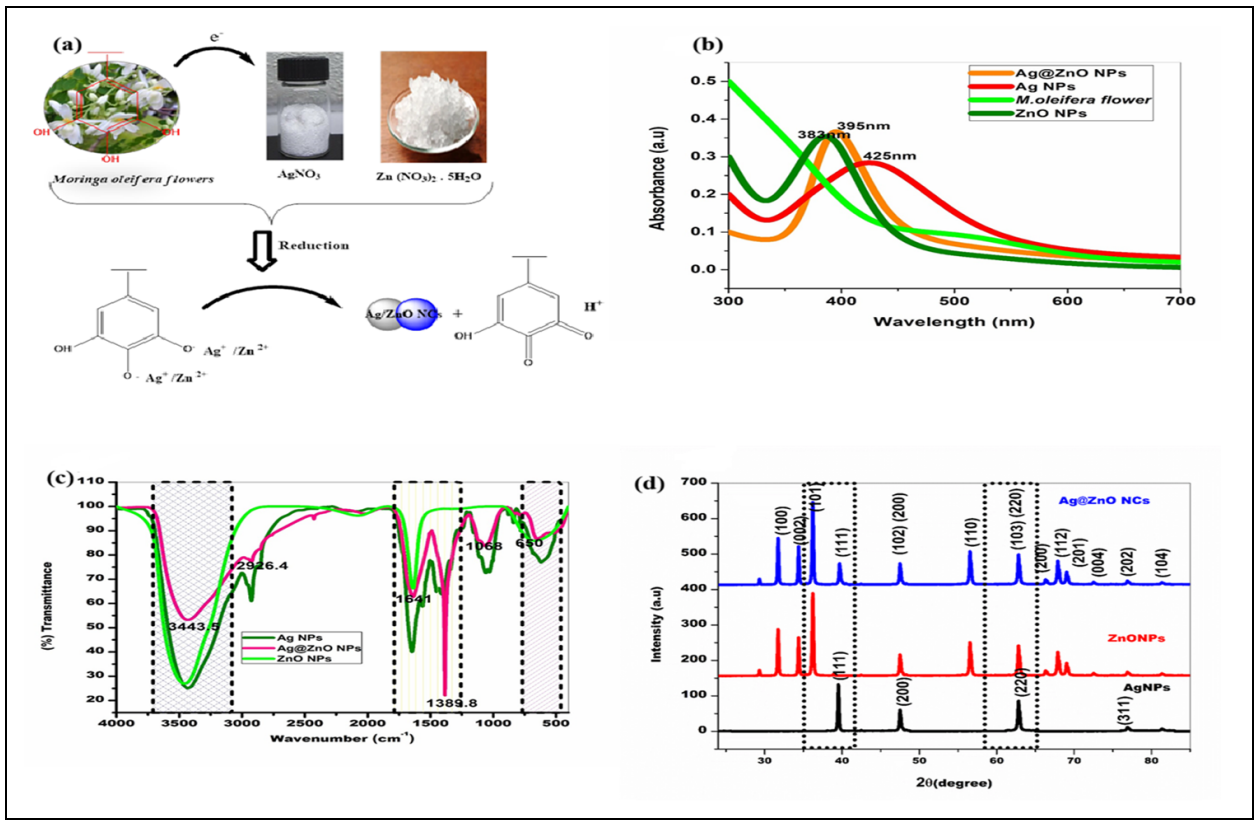


Fig. 1: (a) Preparation method for Ag@ZnO hybrids using *M. oleifera* flower extract, and (b) UV–Vis absorbance spectra, (c) FT-IR spectra and (d) XRD patterns of Ag NPs, ZnO NPs, and Ag@ZnO nanohybrids

3.2 UV–Vis Spectroscopy

The optical properties of the Ag@ZnO nanohybrids were evaluated by using UV–Vis spectroscopy to confirm the formation of Ag NPs. As shown in Fig.1(b), a maximum absorbance at 425 nm was observed, which can be attributed to the SPR of Ag NPs. In addition, the color of the solution changed from light brown to dark brown, indicating the reduction of Ag^{+} to Ag^{0} and the formation of Ag NPs (Ismail *et al.*2018). The Ag NPs remained extremely stable, with no notable modifications in the absorption peak's uniformity, location, or shape even after two months. Fig. 1(b) also displays the absorbance spectrum of the Ag@ZnO hybrids, in which the SPR of the conductive NPs is evident. The absorption edge at about 425 nm is due to the Ag NPs, while the strong absorption border at approximately 383 nm is related to the intrinsic bandgap transitions of the wurtzite hexagonal ZnO structure (Kayani *et al.*2020). Notably, a slight shift in the absorption peak position was observed after the formation of the Ag@ZnO nanohybrids compared with the individual components. This shows that Ag and ZnO have a strong interaction at the interface. This change can be attributed to electronic coupling and charge transfer at the Ag–ZnO interface. Adding Ag also increases the absorption of visible light through the surface plasmon resonance effect, which makes the hybrid nanostructure better at both optical characteristics and catalytic performance.

3.3 FT-IR Analysis

Fig. 1(c) presents the FT-IR spectra of as-prepared Ag NPs, ZnO NPs, and Ag@ZnO nanohybrids using *M. oleifera* flower extract. This suggests that the phenolic compounds were adsorbed onto the hybrid surfaces, likely through π-electron interactions, without significant contributions from other bonding factors (Alprol *et al.*2024; Arun *et al.*2024). Notably, the observed peaks at 3443, 1641, 1389.8, and 1068 cm^{-1}correspond to O–H stretching, carbonyl (C=O) stretching, aromatic C=C stretching, and C-OH stretching vibrations, respectively. Additionally, the band observed at 2926 cm^{-1}denotes the capture of ambient CO_2 by metallic cations. A broad peak in the 650 cm^{-1} region is indicative of Zn-O vibrations, confirming the presence of ZnO in the nanohybrids (Sudha *et al.*2023).

3.4 XRD Analysis

The crystalline nature of the as-prepared materials was analyzed using powder XRD, and the diffraction pattern of the Ag@ZnO hybrid is shown in Fig. 1(d). The diffraction patterns of the synthesized materials, matched against the standard data (JCPDS

Card No.: 80-0075) and aligned closely with the hexagonal wurtzite structure of ZnO. Additionally, the XRD pattern of the Ag@ZnO hybrid displays several new reflections at 2θ = 32.1, 35.6, 37.8, 39.2, 48.4, 57.6, 64.2, 66.2, 67.8, 69.2,72.5, 75.6 and 81.2°, which correspond to the (100), (002), (101), (111), (102), (200), (110), (103),(220), (200), (112), (201), (004), (202) and (104) planes of the face-centered cubic (FCC) structure of immobilized Ag NPs on the ZnO, respectively, according to the standard JCPDS Card No.: 87-0717 (Rabbi *et al.*2024; Nasrollahzadeh *et al.*2021).The presence of these reflections indicates the successful integration of Ag nanoparticles onto the ZnO matrix, confirming the formation of the Ag@ZnO hybrids. The diffraction peaks corresponding to ZnO indicate that its crystalline structure is still maintained even after the incorporation of Ag NPs. This suggests that the synthesis process does not disrupt the ZnO's hexagonal structure, and the observed additional peaks are due to the immobilized Ag NPs, highlighting the composite nature of the material. The distinct peaks corresponding to Ag NPs suggest a well-defined FCC crystal structure, supporting the successful synthesis and potentially enhanced properties of the Ag@ZnO hybrids (Xaviour *et al.*2024). Crystalline size (D) was assessed by using the Debye-Scherrer expression:

$$D = \frac{0.9\lambda}{\beta \cos\theta} \quad \ldots(2)$$

Where λ denotes the frequency of the radiation (Kα = 1.54056 Å), β represents the full width at half maximum (FWHM), and θ is the diffraction angle. The resulting algorithm was used to compute the lattice coefficient (a) estimates of the produced specimens:

$$a = d\sqrt{h^2 + k^2 + l^2} \quad \ldots(3)$$

Where d refers to the interplanar region along with *h, k, and l*, constitute the Miller's constants.

3.5 Microstructural Parameter Measurement

The dislocation density (δ) is associated with structural distortions within the crystalline material, whereas the stacking fault (τ) corresponds to imperfections arising from ZnO incorporation into the Ag lattice structure. These parameters were calculated using Eqs. (4) and (5) (Williamson et al. 1956)

$$\delta = \frac{1}{D^2} \quad \ldots(4)$$

$$\tau = \left[\frac{2\pi r^2}{45(3\tan\theta)^{\frac{1}{2}}}\right]\beta \quad \ldots(5)$$

where r represents the interplanar spacing of the crystal lattice. The X-ray frequency (p_x) associated with the NPs created is calculated roughly as Eq (6):

$$p_x = \frac{4M}{N_a a^3} \ldots(6)$$

whereN_a denotes the Avogadro number (6.022 × 10^{23} mol^{-1}), M represents the molecular mass of the specimen and 'a' corresponds to the lattice parameter of the crystal structure. The computed values are presented in the following Table1.

3.6Size, Shape and Elemental Composition Analysis

The SEM images of as-prepared Ag NPs, ZnO NPs, and Ag@ZnO hybrids show unique and well-defined morphologies, as shown in Fig. 2 (a, c, and e). Ag NPs synthesized by the same green extract method were more spherical in shape, uniform in size, and smooth on the surface, whereas ZnO NPs exhibited a rod-like morphology with elongated structures and a high aspect ratio (Ghosh *et al.*2014). Ag@ZnO hybrids were synthesized by integrating spherical Ag NPs with rod-like ZnO, and they have shown a unique rod-like spherical morphology. This combination results in a mixture with a cohesive structure, revealing spherical Ag NPs dispersed on the surface of ZnO rods.SEM images confirmed the successful green synthesis of nanocomposites by demonstrating the effectiveness of *M. oleifera* flower extract in forming high-quality nanocomposites and its ability to form various nanostructures for various applications. Energy-dispersive X-ray (EDX) spectroscopy analysis revealed the presence of Ag, Zn, and O elements, as depicted in Fig. 2 (b, d, and f).

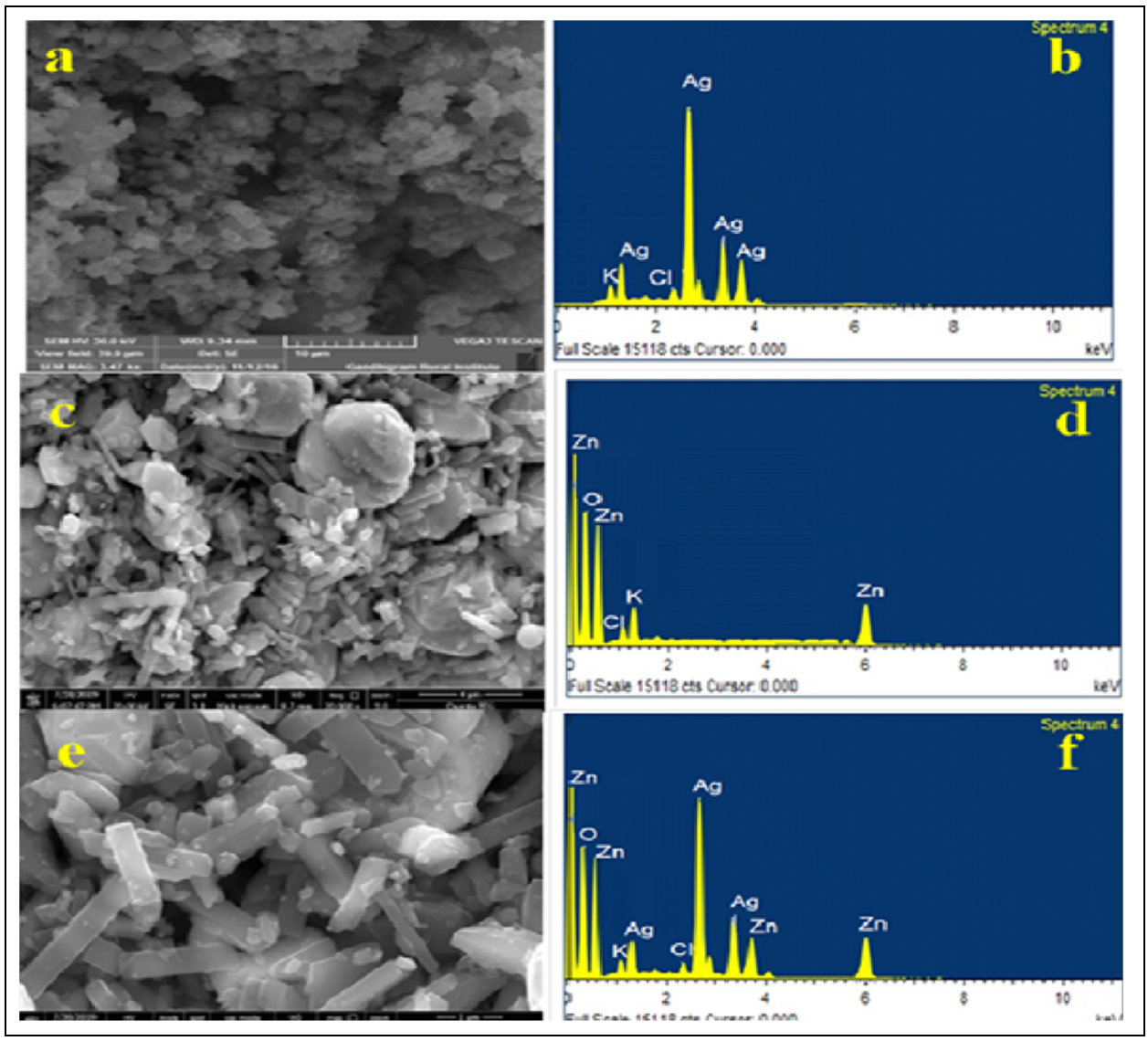


Fig. 2: (a, c, and e) SEM micrographs and (b, d, and f) EDX profile of Ag NPs, ZnO NPs and Ag@ZnO hybrids, respectively

3.7 Evaluation of the Reduction of MO Dye

The catalytic activity of Ag NPs, ZnO NPs, and Ag@ZnO hybrid nano structure in the removal of MO using $NaBH_4$ is notable due to their varying efficiencies and mechanisms. The tested Ag NPs exhibited a rapid reduction and achieved~97.6% removal in just 13 min. ZnO species were slightly slower but still effective, reaching ~94.6% removal in 17 min (Nisha *et al.*2025). The Ag@ZnO hybrids demonstrated exceptional catalytic performance, achieving 99.8% removal within 8 min, showcasing synergistic effects between Ag and ZnO, as shown in Fig. 3 (a, c, and e). The Ag@ZnO hybrid nanostructure exhibited significantly enhanced degradation efficiency compared to individual Ag and ZnO nanoparticles, which can be attributed to the synergistic interaction between the two components. The presence of Ag NPs on the ZnO surface facilitates efficient electron trapping and transfer, thereby suppressing the recombination of photogenerated electron–hole pairs. Furthermore, the formation of a Schottky barrier at the Ag–ZnO interface enhances charge separation and prolongs the lifetime of charge carriers. This process promotes the generation of reactive oxygen species such as hydroxyl radicals (•OH) and superoxide radicals ($O_2^{\bullet -}$), which actively participate in the degradation of dye molecules. In addition, the improved surface area and active sites in the hybrid structure further contribute to the accelerated catalytic activity, resulting in faster degradation compared to individual nanoparticles. In addition, control experiments without catalysts showed negligible activity, confirming the necessity of catalysts for efficient dye reduction. The initial addition of a small amount of $NaBH_4$ slightly decreased efficiency but subsequently accelerated the reduction process when combined with nanohybrids. The slight initial decrease in efficiency can be attributed to the induction period

required for the adsorption of dye molecules and BH_4^- ions onto the catalyst surface. During this stage, the electron transfer pathway is gradually established. Once this interaction is stabilized, $NaBH_4$ acts as a strong reducing agent, resulting in a rapid increase in the degradation rate. This improvement is ascribed to an electro-relay effect facilitated by the catalysts, underscoring their role in accelerating the MO dye reduction process (Tan *et al.*2024). A kinetic model was used to assess the rate of decomposition of MO dye using Ag NPs, ZnO NPs, and Ag@ZnO hybrid. The rate constant (k_{app}) was determined by the relevant kinetic equation (Eq. 7).

$$ln\left(\frac{C_0}{C_t}\right) = -k_{app}t \qquad \ldots(7)$$

where k_{app} indicates the rate constant of the catalytic reaction, C_0represents the initial concentration of the dye, and C_t indicates the concentration of the dye at time t for MO. The catalyst breakdown of MO dye substantially adheres to first-order kinetics, as shown in Fig.3 (Ouyang *et al.*2020). From Eq. (7), the k_{app} values are 0.0321 min^{-1}, 0.0425 min^{-1}, and 0.0021 $min^{-1}$for Ag NPs, ZnO NPs, and Ag@ZnO hybrids, respectively, as shown in Fig. 3 (b, d, and f).

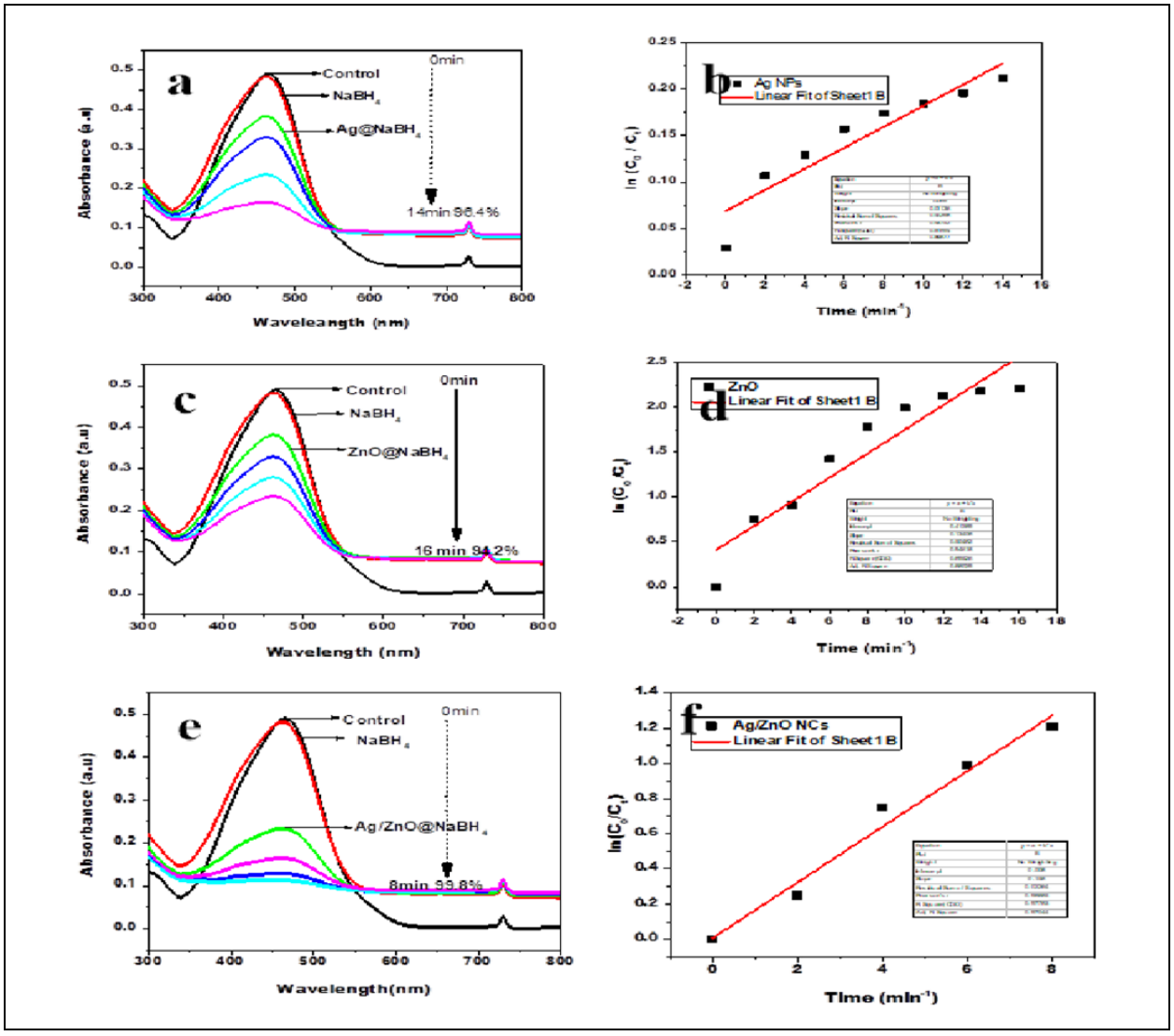


Fig. 3: UV–Vis absorption spectra of MO removal on (a) Ag NPs, (c) ZnO NPs and (e) Ag@ZnO hybrids; (b, d, and f) their corresponding kinetic plots

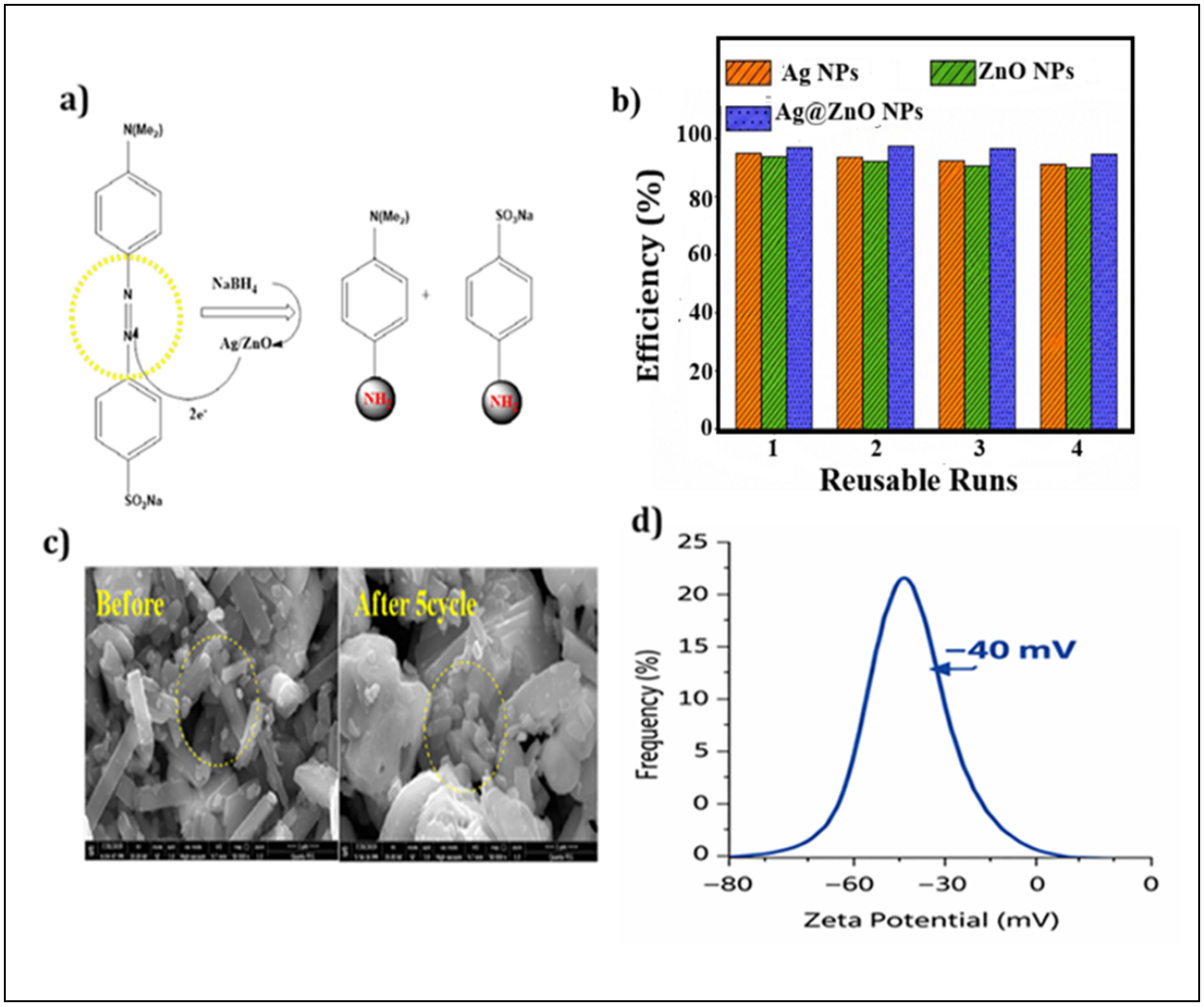


Fig. 4: (a) Catalytic removal mechanism of MO by Ag@ZnO hybrids using $NaBH_4$, (b) recyclability test for MO removal using Ag, ZnO, and Ag@ZnO nanohybrids, (c) stability of Ag@ZnO nano hybrids before and after the fifth recycling cycle, and(d) zeta-potential distribution of the synthesized Ag@ZnO hybrid nanostructure, showing a peak around −40 mV

3.8 Catalytic Mechanism

The catalytic mechanism of MO elimination on Ag@ZnO hybrid nano structure using $NaBH_4$ typically involves multiple steps. Initially, Ag NPs on the ZnO surface act as catalytic sites where $NaBH_4$ undergoes hydrolysis to produce hydrogen gas and $BH_3(OH)$, which acts as a reducing agent. $BH_3(OH)$ then interacts with the Ag NPs, facilitating the reduction of MO molecules (Fig. 4 (a)). This reduction process involves the transfer of electrons from $BH_3(OH)$ to the MO molecules adsorbed on the Ag@ZnO hybrid surface, resulting in the formation of less colored or colorless products, indicating degradation of the MO dye. The synergistic effect between Ag NPs and ZnO provides enhanced catalytic activity by promoting electron transfer and stabilizing reactive intermediates, thereby facilitating the effective elimination of MO in aqueous solutions (Vaez *et al.*2020; Nisha *et al.*2023).

3.9 Recyclable Assessment

The reusability of unconventional catalysts makes them suitable for industrial applications. Despite a slight decrease in catalytic activity, the Ag@ZnO nanohybrids could be readily recovered from the reaction mixture and reused for five consecutive cycles of dye degradation. The catalytic performance remained relatively stable up to the fifth cycle, and the time required to achieve complete degradation remained nearly constant throughout the recycling process (Fig. 4b). This demonstrates the high stability and reusability of the catalyst under practical application conditions (Rajeswaran *et al.*2026).

3.10 Stability of Ag@ZnO Hybrids

Recycling of Ag@ZnO hybrids in MO dye reduction process was investigated, and it was exhibited that the catalyst has good stability, can be recycled and

reused five times, and has a low cost. Similarly synthesized Ag@ZnO hybrid catalyst remained stable up to the fifth cycle (Fig. 4(c). The FE-SEM image of Ag@ZnO hybrids shows a slight change in size, shape, or chemical composition after five catalytic runs. Zeta-potential analysis was carried out to further evaluate the stability of the synthesized nanoparticles (Fig. 4d). The Ag@ZnO combination demonstrated a zeta potential of roughly –40 mV, signifying exceptional colloidal stability. The high negative surface charge generates significant electrostatic repulsion among the particles, thereby inhibiting agglomeration and promoting uniform dispersion. This result strongly supports the observed stability of the catalyst during several degrading cycles.

3.11 Comparison with Previous Studies

The catalytic efficacy of the prepared Ag@ZnO composite was subsequently assessed against previously reported catalysts for the decomposition of MO. Pristine ZnO NPs typically demonstrate low degradation efficiency owing to the fast recombination of photogenerated charge carriers (Kumar *et al.*2017). Numerous studies have shown that the addition of Ag to ZnO markedly improves catalytic activity by facilitating charge separation and enhancing visible light absorption via SPR (Singh *et al.*2018). Specifically, Ag/ZnO nanocomposites synthesized by environmentally friendly methods have demonstrated degradation efficiencies between 85% and 95% for MO under comparable settings (Ismail *et al.*2018; Kayani *et al.*2020). In contrast, the current Ag@ZnO hybrid nanostructure demonstrates superior degrading efficiency and accelerated reaction kinetics, attributable to the robust interfacial connection between Ag and ZnO, augmented electron transport, and heightened accessibility of active sites. The results validate that the synthesized hybrid nanostructure exhibits excellent efficiency and competes favorably with previously reported catalysts for wastewater treatment applications.

4. CONCLUSION

In the present study, a green method for synthesizing Ag NPs, ZnO NPs, and Ag@ZnO hybrids using *M. Oleifera* flower extract was developed, and the synthesized materials were characterized using various analytical techniques. The nanoparticles demonstrated significant effectiveness in the degradation of MO dye, with Ag NPs, ZnO NPs, and Ag@ZnO hybrid achieving 97.6% degradation within17 min, 94.6% within13 min, and 99.8% within8 min, respectively. The superior performance of the Ag@ZnO hybrids was attributed to their rapid electron-transfer process, which enhanced catalytic activity compared with the individual catalysts. A significant outcome of this study is the demonstrated potential of these nanoparticles as effective catalysts for water-treatment applications. The ability of the Ag@ZnO nanohybrids to maintain high catalytic activity over multiple reuse cycles further emphasizes their practical applicability and stability. This durability suggests broader applicability of these materials not only for dye degradation but also for the removal of various other contaminants, thereby contributing to the development of sustainable environmental-remediation technologies.

AUTHOR CONTRIBUTIONS

V. Subha, R. Kayalvizhi, and M. Nagoor Meeran: Study conceptualization and writing the manuscript; S. Kalpana, and R. Nagalakshmi: Data curation, formal analysis, and writing (review and editing).

DATA AVAILABILITY STATEMENT

The data that support the findings of this study are available from the corresponding author upon reasonable request.

ACKNOWLEDGEMENT

The authors are grateful to Vel Tech Rangarajan Dr. Sagunthala R&D Institute of Science and Technology (Deemed University), Chennai, Tamilnadu, India, for providing the facilities to conduct the research work.

FUNDING

This research received no specific grant from any funding agency in the public, commercial, or not-for-profit sectors.

CONFLICTS OF INTEREST

The authors declare that there is no conflict of interest.

COPYRIGHT

This article is an open-access article distributed under the terms and conditions of the Creative Commons Attribution (CC BY) license (http://creativecommons.org/licenses/by/4.0/).



REFERENCES

Akhtar, K., Ali, F., Sohni, S., Kamal, T., Asiri, A. M., Bakhsh, E. M. and Khan, S. B., Lignocellulosic biomass supported metal nanoparticles for the catalytic reduction of organic pollutants, *Environ. Sci. Pollut. Res.*, 27(1), 823-836(2020). https://doi.org/10.1007/s11356-019-06908-y

Alprol, A. E., Eleryan, A., Abouelwafa, A., Gad, A. M. and Hamad, T. M., Green synthesis of zinc oxide nanoparticles using Padina pavonica extract for efficient photocatalytic removal of methylene blue, *Sci. Rep.*, 14(1), 32160(2024). https://doi.org/10.1038/s41598-024-80757-9

Alzahrani, E. A., Nabi, A., Kamli, M. R., Albukhari, S. M., Althabaiti, S. A., Al-Harbi, S. A., Khan, I. and Malik, M. A., Facile green synthesis of ZnO NPs and plasmonic Ag-supported ZnO nanocomposite for photocatalytic degradation of methylene blue, *Water*, 15(3), 384(2023). https://doi.org/10.3390/w15030384

Arun,K. T., Sangeethapriya, S., Kiruthikha, M. and Rajeswaran, P., Facile green synthesis of Sm_2O_3@ g–C_3N_4 for enhanced photocatalytic and catalytic degradation of organic pollutant, *J. Mater. Sci.: Mater. Electron.,* 35(28), 1842 (2024). https://doi.org/10.1007/s10854-024-13638-6

Aththanayaka, S., Thiripuranathar, G. and Ekanayake, S., Microwave-assisted phytogenic Ag/Ag_2O/ZnO nanocomposite as a replacement of Ag/Ag_2O and ZnO nanoparticles: A comparative antioxidant study, *Surf. Interf.*, 43, 103547 (2023). https://doi.org/10.1016/j.surfin.2023.103547

Bavykina, A., Kolobov, N., Khan, I. S., Bau, J. A., Ramirez, A. and Gascon, J., Metal–organic frameworks in heterogeneous catalysis: recent progress, new trends, and future perspectives, *Chem. Rev.,* 120(16), 8468–8535 (2020). https://doi.org/10.1021/acs.chemrev.9b00685

Bi, T., Du, Z., Chen, S., He, H., Shen, X. and Fu, Y., Preparation of flower-like ZnO photocatalyst with oxygen vacancy to enhance the photocatalytic degradation of methyl orange, *Appl. Surf. Sci.*, 614, 156240 (2023). https://doi.org/10.1016/j.apsusc.2022.156240

Bloch, K., Mohammed, S. M., Karmakar, S., Shukla, S., Asok, A., Banerjee, K., Patil-Sawant, R., Mohd Kaus, N. H., Thongmee, S. and Ghosh, S., Catalytic dye degradation by novel phyto fabricated silver/zinc oxide composites, *Front. Chem.*, 10, 1013077 (2022), https://doi.org/10.3389/fchem.2022.1013077

Donkadokula, N. Y., Kola, A. K., Naz, I. and Saroj, D., A review on advanced physico-chemical and biological textile dye wastewater treatment techniques, *Rev. Environ. Sci. Biotechnol.*, 19(3), 543–560 (2020). https://doi.org/10.1007/s11157-020-09543-z

Ghosh, M., Karmakar, D., Basu, S., Jha, S. N., Bhattacharyya, D., Gadkari, S. C. and Gupta, S. K., Effect of size and aspect ratio on structural parameters and evidence of shape transition in zinc oxide nanostructures, *J. Phys. Chem. Solids.*, 75(4), 543-549 (2014). https://doi.org/10.1016/j.jpcs.2013.11.007

Islam, T., Repon, M. R., Islam, T., Sarwar, Z. and Rahman, M. M., Impact of textile dyes on health and ecosystem: a review of structure, causes, and potential solutions, *Environ. Sci. Pollut. Res.*, 30(4), 9207-9242(2022). https://doi.org/10.1007/s11356-022-24398-3

Ismail, M., Akhtar, K., Khan, M. I., Kamal, T., Khan, M. A. M., Asiri, A., Seo, J. and Khan, S. B., Pollution, toxicity and carcinogenicity of organic dyes and their catalytic bio-remediation, *Curr. Pharm. Des.,* 25(34), 3645-3663 (2019). https://doi.org/10.2174/1381612825666191021142026

Ismail, M., Khan, M. I., Akhtar, K., Khan, M. A., Asiri, A. M. and Khan, S. B., Biosynthesis of silver nanoparticles: A colorimetric optical sensor for detection of hexavalent chromium and ammonia in aqueous solution, *Physica E: Low-dimension. Syst. Nanostruct.*, 103, 367-376 (2018). https://doi.org/10.1016/j.physe.2018.06.015

Janaki, K., Saravanan, S. and Sankara, R. N., Study of antimicrobial performance of green synthesized TiO_2 nanostructures, *J. Environ. Nanotechnol.,* 14(4), 136–142 (2025). https://doi.org/10.13074/jent.2025.12.2541894

Kayani, Z. N., Manzoor, F., Zafar, A., Mahmood, M., Rasheed, M. and Anwar, M., Impact of Ag doping on structural, optical, morphological, optical and photoluminescent properties of ZnO nanoparticles, *Opt. Quantum Electron.*, 52(7), 344 (2020). https://doi.org/10.1007/s11082-020-02460-z

Khan, Z. U. H., Khan, A., Shah, A., Wan, P., Chen, Y., Khan, G. M., Khan, A. U., Tahir, K., Muhammad, N. and Khan, H.U., Enhanced photocatalytic and electrocatalytic applications of green synthesized silver nanoparticles, *J. Mol. Liq*., 220, 248-257 (2016). https://doi.org/10.1016/j.molliq.2016.04.082

Khanam, Z., Sultana, F. M. and Mushtaq, F., Environmental pollution control measures and strategies: an overview of recent developments, *Geospa. Anal. Environ. Pollut. Model.,* 385-414 (2023). https://doi.org/10.1007/978-3-031-45300-7_15

Koul, B., Bhat, N., Abubakar, M., Mishra, M., Arukha, A. P. and Yadav, D., Application of natural coagulants in water treatment: a sustainable alternative to chemicals, *Water*, 14(22), 3751 (2022). https://doi.org/10.3390/w14223751

Kumar, R., Umar, A., Kumar, G. and Nalwa, H. S., Antimicrobial properties of ZnO nanomaterials: A review, *Ceram. Int.,* 43(5), 3940-3961 (2017). https://doi.org/10.1016/j.ceramint.2016.12.062

Kumar, T. A., Ramkumar, J., Kiruthikha, M. and Rajeswaran, P., Green synthesis and characterization of $SmVO_4$@ g-C_3N_4 with investigation of photocatalytic and antioxidant activities, *Waste Biomass Valorization*, 16(7), 3631-3646 (2025). https://doi.org/10.1007/s12649-025-02886-0

Meyyarasan, K., Kavitha, S., Venkatesa, P. S. and Saravanan, S., Enterobacter cloacae Cell Lysate-mediated Biosynthesis of AgNPs: Physicochemical Characterization and Bactericidal Kinetics, *J. Environ. Nanotechnol.,* 14(4),238-247 (2025).https://doi.org/10.13074/jent.2025.12.2541803

Nasrollahzadeh, M., Shafiei, N., Soleimani, F., Nezafat, Z. and Bidgoli, N. S., Physicochemical characterization of biopolymer-based metal nanoparticles, *Biopolym. Met. Nanopart. Chem. Sustain. Appl.*, 317-478 (2021). https://doi.org/10.1016/b978-0-12-822108-2.00017-x

Naz, M., Rafiq, A., Ikram, M., Haider, A., Ahmad, S. O. A., Haider, J. and Naz, S., Elimination of dyes by catalytic reduction in the absence of light: A review, *J. Mater. Sci.*, 56(28), 15572-15608 (2021). https://doi.org/10.1007/s10853-021-06279-1

Nisha, U. M., Meeran, M. N., Sethupathi, R., Subha, V., Rajeswaran, P. and Sivakarthik, P., Studies on Chitosan modified ZrO_2–CeO_2 metal oxide and their Photo catalytic activity under solar light irradiation for water remediation, *J. Indian Chem. Soc.*, 100(8), 101061 (2023). https://doi.org/10.1016/j.jics.2023.101061

Nisha, U. M., Venkatesh, D., Vasanthan, S., Rajeswaran, P., Balaji, J. and Karthik, P. S., Interfacial coupling effects of chitosan integrated ZrO_2/Bi_2O_3/CeO_2 quaternary composite for efficient wastewater treatment and antimicrobial activity, *Ionics*, 31(3), 2739-2756 (2025). https://doi.org/10.1007/s11581-025-06095-6

Parashar, M., Shukla, V. K. and Singh, R., Metal oxides nanoparticles via sol–gel method: a review on synthesis, characterization and applications, *J. Mater. Sci.: Mater. Electron.*, 31(5), 3729-3749 92020). https://doi.org/10.1007/s10854-020-02994-8

Rabbi, M. B. U., Haque, S. and Bedoura, S., Advancements in synthesis, immobilization, characterization, and multifaceted applications of silver nanoparticles: A comprehensive review, *Heliyon*, 10(24), e40931(2024). https://doi.org/10.1016/j.heliyon.2024.e40931

Rajeswaran, P., Balaramesh, P., Vijayakumar, B., Muralidharan, V. P., Subha, V. and Selvarani, V., Ficus carica Fruit Extract Mediated Synthesis of ZrO2 Nanoparticles for Enhanced Photocatalytic Degradation and Environmental Remediation, *Waste Biomass Valorization*, 17(1), 85-99 (2026). https://doi.org/10.1007/s12649-025-03097-3

Rajeswaran, P., Kamalarajan, P., Vasanthan, S., Sivagami, S., Venkatesh, D. and Karthik, P. S., Structural elucidation and environmental remediation potential of novel $CoMn_2O_4$@ rGOnano catalyst. *J. Inorg. Organomet. Polym. Mater.*, 35(9), 7920-7933 (2025a)
https://doi.org/10.1007/s10904-025-03741-4

Rajeswaran, P., Raja, G., Raja, M., Sunderraj, A. G. and Umavathy, K., Structural elucidation and environmental remediation potential of novel NiCoP@ rGOnanocatalyst,*DiamondRelat. Mater.*, 154, 112123 (2025b). https://doi.org/10.1016/j.diamond.2025.112123

Saleh, H. M. and Hassan, A. I., Synthesis and characterization of nanomaterials for application in cost-effective electrochemical devices, *Sustainability,* 15(14), 10891 (2023). https://doi.org/10.3390/su151410891

Sanjeev, N. O., Gupta, N. V. and Mbuya, V. B., Synthesis of zinc oxide nanoparticles from Azadirachta indica extract for wastewater treatment, *J. Hazard. Toxic Radioact. Waste*, 27(4), 04023027 (2023). https://doi.org/10.1061/jhtrbp.hzeng-1217

Sathish, T., Kumar, S. and Rajendran, V., A facile synthesis of Ag/ZnO nanocomposites prepared via green route for catalytic activity, *Appl. Phys. A*, 127(9), 692 (2021). https://doi.org/10.1007/s00339-021-04854-6

Shahzadi, S., Fatima, S., Shafiq, Z., and Janjua, M. R. S. A., A review on green synthesis of silver nanoparticles (SNPs) using plant extracts: a multifaceted approach in photocatalysis, environmental remediation, and biomedicine. *RSC Adv., 15*(5), 3858-3903 (2025). https://doi.org/10.1039/d4ra07519f

Sharma, R. K., Yadav, S., Dutta, S., Kale, H. B., Warkad, I. R., Radek, Z., Varma, R. S., Gawande, M. B. and Varma, R. S., Silver nanomaterials: synthesis and catalytic applications, *Chem. Soc. Rev*., 50(20), 11293–11380 (2021). https://doi.org/10.1039/d0cs00912a

Singh, J., Dutta, T., Kim, K. H., Rawat, M., Samddar, P. and Kumar, P., Green' synthesis of metals and their oxide nanoparticles: applications for environmental remediation, *J. Nanobiotechnol.,* 16(1), 84 (2018). https://doi.org/10.1186/s12951-018-0408-4

Sudha, D., Kumar, E. R., Shanjitha, S., Munshi, A. M., Al-Hazmi, G. A., El-Metwaly, N. M., and Kirubavathy, S. J., Structural, optical, morphological and electrochemical properties of ZnO and graphene oxide blended ZnO nanocomposites, *Ceram. Int.*, 49(5), 7284-7288 (2023). https://doi.org/10.1016/j.ceramint.2022.10.192

Tan, C., Yin, Y., Zuo, J. and Li, J., Preparation and photocatalytic properties of Bi_2WO_6/Ag/ZnO composite nanomaterials, *Int. J. Quantum Chem.*, 124(9), e27380 (2024). https://doi.org/10.1002/qua.27380

Tashi, T., Gupta, N. V. and Mbuya, V. B., Silver nanoparticles: Synthesis, mechanism of antimicrobial action, characterization, medical applications, and toxicity effects, *J. Chem. Pharm. Res*, 8(2), 526-537 (2016). https://doi.org/10.1186/2228-5326-2-32

Uddin, N., Zhang, H., Du, Y., Jia, G., Wang, S. and Yin, Z., Structural-phase catalytic redox reactions in energy and environmental applications, *Adv. Mater.*, 32(9), 1905739 (2020).https://doi.org/10.1002/adma.201905739

Uribe-López, M. C., Hidalgo-López, M. C., López-González, R., Frías-Márquez, D. M., Núñez-Nogueira, G., Hernández-Castillo, D. and Alvarez-Lemus, M. A., Photocatalytic activity of ZnO nanoparticles and the role of the synthesis method on their physical and chemical properties, *J. Photochem. Photobiol. A: Chem.*, 404, 112866 (2021). https://doi.org/10.1016/j.jphotochem.2020.112866

Usliyanage, J. P., Perera, G., Thiripuranathar, G. and Menaa, F., Synthetic strategies of Ag-doped ZnO nanocomposites: a comprehensive review. *Biomass Convers. Biorefin.*, 15(1), 19-39 (2025). https://doi.org/10.1007/s13399-023-05139-z

Vaez, Z. and Javanbakht, V., Synthesis, characterization and photocatalytic activity of ZSM-5/ZnO nanocomposite modified by Ag nanoparticles for methyl orange degradation, *J. Photochem. Photobiol. A: Chem.*, 388, 112064 (2020). https://doi.org/10.1016/j.jphotochem.2019.112064

Veeramalli, N. S., Aravind, K. J., Leena, R. R., Anbarasan, P., Gomathi, S. and Vasamsetti, S. S., Fabrication of Activated Carbon-HKUST-1 MOF Nanocomposites for Enhanced Adsorption and Decontamination of Acidic and Basic Dyes in Wastewater, *J. Environ. Nanotechnol.,* 14(4), 192-208 (2025). https://doi.org/10.13074/jent.2025.12.2541842

Venkatesh, D., Kanchana, V., Vasanthan, S., Kistan, A., Rajeswaran, P., Arunkumar, K. and Karthik, P. S., Design and fabrication of magnetically recoverable $SnO_2/CoFe_2O_4$ nanocomposite for enhanced visible light-driven wastewater treatment, *Inorg. Chem. Commun.*, 166, 112657 (2024). https://doi.org/10.1016/j.inoche.2024.112657

Wafi, A. and Mohammad, M. K., Green synthesized ZnO and ZnO-based composites for wound healing applications, *Bioprocess Biosyst. Eng*., 48(4),521-542(2025). https://doi.org/10.1007/s00449-024-03123-z

Williamson, G. K. and Smallman, R. E., III. Dislocation densities in some annealed and cold-worked metals from measurements on the X-ray Debye–Scherrer spectrum: *Philos. Mag.,* 1(1), 34–46 (1956). https://doi.org/10.1080/14786435608238074

Xaviour, J., Sreelekshmi, S., Joseph, J., Fathima, S. A. and Sajini, T., Eco-friendly synthesis and enhanced antibacterial action of bimetallic Ag/ZnO nanoparticles using Hylocereus costaricensis stem extract, *RSC Sustainability,* 2(10), 3077-3089 (2024). https://doi.org/10.1039/d4su00254vg

Xie, S., Yang, Y., Gai, W. Z. and Deng, Z. Y., Oxide modified aluminum for removal of methyl orange in aqueous solution, *RSC Adv.,* 11(2), 867–875 (2021).https://doi.org/10.1039/d0ra09048d

Zhang, S., Chen, J., Ma, Y., Zhao, Q., Jing, B., Yu, M., Yang, N., Yang, A., Shen, Q., Wang, Y., Zhao, C. and Yang. H., Green synthesis, biomedical effects, and future trends of Ag/ZnO bimetallic nanoparticles: *Nanotechnol. Rev.,* 14(1), 20250186 (2025). https://doi.org/10.1515/ntrev-2025-0186